Exploiting Adaptive and Collaborative AUV Autonomy for Detection and Characterization of Internal Waves

Exploiting Adaptive and Collaborative AUV Autonomy for Detection and Characterization of Internal Waves

Stephanie Petillo, *Student Member, IEEE,* and Henrik Schmidt

Abstract

Advances in the fields of autonomy software and environmental sampling techniques for autonomous underwater vehicles (AUVs) have recently allowed for the merging of oceanographic data collection with the testing of emerging marine technology. The Massachusetts Institute of Technology (MIT) Laboratory for Autonomous Marine Sensing Systems (LAMSS) group conducted an Internal Wave Detection Experiment in August 2010 with these advances in mind. The goal was to have multiple AUVs collaborate autonomously through on board autonomy software and real-time underwater acoustic communication to monitor for the presence of internal waves by adapting to changes in the environment (specifically the temperature variations near the thermocline/pycnocline depth). The experimental setup, implementation, data, deployment results, and internal wave detection and quantification results are presented in this paper.

Index Terms

Adaptive systems, Autonomous underwater vehicles, Oceanic engineering and marine technology, Sampling methods, Robot sensing systems

Manuscript received October 31, 2011; revised October 04, 2012.

This work was supported by the U.S. Office of Naval Research N00014-08-1-0013 and by Government support under and awarded by DoD, Air Force Office of Scientific Research, National Defense Science and Engineering Graduate (NDSEG) Fellowship, 32 CFR 168a.

The authors are with the Massachusetts Institute of Technology, Cambridge, MA 02139 USA; S. Petillo is also with the Woods Hole Oceanographic Institution, Woods Hole, MA 02543 USA (e-mail: spetillo@mit.edu; henrik@mit.edu).

I. INTRODUCTION

Bodies of water in nature tend to be stably stratified with fluid density increasing with depth. This density variation is dependent upon water temperature, salinity, and pressure through the equation of state for seawater [1]. When an abrupt change in water density occurs over a short depth range, often referred to as a pycnocline, the boundary between the two layers of different-density seawater may support internal waves. That is, the strongly stable stratification of the density layers at the pycnocline will react with a restoring force when perturbed by water from above being forced downward or water from below being forced upward, creating an internal wave that will propagate away from its source along an isopycnal within the pycnocline [2]. Perturbations from internal waves can occur from a variety of sources, such as currents flowing rapidly past a narrow mouth to a basin, or waves produced by flow over underwater mountains or canyons near a shelf break. Internal waves frequently occur in regions where a strong thermocline is present and salinity can be considered constant (the pycnocline depth will then be coincident with that of the thermocline in shallow water).

Internal waves have a strong effect on acoustic propagation in any body of water, since sound waves travel as pressure waves that can be refracted in different directions as the acoustic impedance of the water changes. Acoustic propagation is used in oceanography for a variety of tomographic experiments and for underwater communication and data transfer when collecting data with autonomous underwater vehicles (AUVs). If the acoustic channel is disturbed by an undetected internal wave, errors in tomographic measurements and unpredicted loss of communication or data transfer to and from AUVs can result.

More specific to the field of oceanography, internal waves of large anplitude and long wavelength relative to water depth can transport a significant amount of energy from one location to another, and those that grow large enough to break along an isopycnal result in mixing between density layers and potential transport of biomass. Internal waves that propagate long distances shed light on the strength of currents and topography interacting both far from coastlines and right off the continental shelf.

In defense applications, detecting the presence of internal waves in an area may reveal the location of a submerged submarine, which generates internal waves through its motion underwater. Internal waves also interact with the acoustic propagation environment during target

(mine) detection and ASW (anti-submarine warfare) operations, causing unpredicted bending in the path of propagating sound waves and thereby (possibly) revealing or concealing potential targets by insonifying an unpredicted area.

Until recently, most field studies of internal waves have been carried out using synthetic aperture radar (SAR) [3]–[5], acoustic tomography and altimetry [6], current meters on moorings [7], CTD (conductivity-temperature-depth) and XBT (expendable bathythermograph) casts [7], and satellite observations (photographs in varying light spectra) [8]. The goal of our experiment, however, was to use AUVs to determine if internal waves were present in our deployment region (more specifics are found in Sections II and III). The specific AUVs for this experiment are actively propelled and able to sense and adapt to their local environment using on board CT (conductivity-temperature) and pressure sensors, along with a computer running autonomy software that can process the data and adaptively redirect the vehicle without an operator in the loop. The choice to use AUVs rather than satellite data, moorings, or CTD casts from a ship for this experiment gave us the flexibility to capture the exact data set we needed using the AUVs' abilities to conduct autonomous and adaptive environmental sampling in real-time, such as thermocline tracking (the thermocline and pycnocline depths are coincident in our AUVs' shallow-water operations region). Autonomous coordination is also possible between multiple AUVs, allowing (in this case) one AUV to travel at the pycnocline depth to collect a data set that is likely to contain internal waves while the other AUV travels well below the pycnocline along the same horizontal track as the first AUV to collect a 'ground truth' data set where internal waves are unlikely to occur.

Using AUVs for internal wave detection is a relatively novel approach. However, the approach presented here is not the first to employ AUVs for this task. Work was done by Zhang et al. in 2001 [9] on spectral classification of internal waves based on vertical flow velocity data from an AUV-mounted ADV (acoustic Doppler velocimeter) during the 1998 Labrador Sea Convection Experiment. In that experiment, the AUV was driven in a predetermined horizontal square pattern at two depths in the upper mixed layer to collect data, which was processed and compared with spectra from an ocean model of the Labrador Sea region containing internal waves. Although no internal waves were found in the vertical velocity spectra, results suggest that significant convection was present in the experimental region. Work has also been done by Cazenave in his 2008 Master's thesis [10] on internal wave detection using the CTD sensor on an AUV,

similarly examining the temperature spectra. Cazenave's experiment took place throughout 2007 in Monterey Bay, CA, through which energetic internal waves are known to pass daily (they have been imaged by satellite). He uses a single AUV that follows a predefined track line between two waypoints in horizontal space while yo-yoing in depth around a set temperature range that is expected to traverse the thermocline in depth. Perturbations in the isotherms and spectral analysis were then used to quantify the internal waves.

Our approach is similar to Cazenave's (and different from that of Zhang et al.) in that it uses CT and pressure data, since CTD (or CT and pressure) sensors are standard on most AUVs. The primary difference from the experiments of Cazenave and Zhang et al. lies in our adaptive and autonomous approach to sampling the environment, and by using multiple AUVs in collaboration to capture synoptic data sets. Also, instead of looking for characteristic vertical velocity modes of internal waves predicted by ocean models (as this will vary from one body of water to the next and requires learning and running an ocean model specific to each location) as done in [9], we take a direct signal processing approach similar to that in [10] to detect the primary frequencies and wavelengths of any potential internal waves propagating along the thermocline interface. In the experiment described below, we have essentially taken Cazenave's thesis work and implemented much of what he saw as future work to make internal wave sampling with AUVs more autonomous, collaborative, and environmentally adaptive.

On 13 August, 2010, we conducted the Internal Wave Detection Experiment (a single-day experiment in the larger GLINT '10 experiment) in the northern coastal basin of the Tyrrhenian Sea bordered by the Tuscan Archipelago and the western coast of Italy (see Fig. 1). Based on historical satellite data and basic bathymetric data from this region in the summer, we expected to see a water depth of less than 200 m in the operation region shown in Fig. 1 (it was actually about 110 m deep there) and sea surface temperatures of about 24 °C with temperatures around 20 °C at 20 m depth and around 14 °C near the sea floor, suggesting summertime stratification that had the potential to sustain internal waves [11]–[13]. According to Turner [2], internal waves propagating along the oceanic thermocline typically have periods of a few minutes, whereas deep ocean internal waves may have periods of up to many hours. Thus, we expect to see internal waves with periods of a few minutes along the thermocline in the Tyrrhenian Sea. This location was chosen due to the availability of ship and AUV resources already deployed for the longer GLINT '10 AUV autonomy experiments. In addition, when researching the possibility of internal

waves in the Tuscan Archipelago basin, all but one scientist we spoke to at the NATO Undersea Research Centre (NURC) in La Spezia, Italy, claimed that we were unlikely to observe any internal waves in the basin, but none could provide any evidence for this. We also found no published literature on the subject of the presence of internal waves in the Tuscan Archipelago basin and thus decided to conduct the Internal Wave Detection Experiment there.

During the Internal Wave Detection Experiment, we were able to demonstrate the use of multiple AUVs communicating (fully through acoustic communication while submerged) and interacting with each other and the environment autonomously in real-time to collect a synoptic environmental data set. The resulting environmental data set would be otherwise incomplete using only one AUV. The two AUVs that were used each belonged to a different research group and were of different manufacture. Thus, we were also able to demonstrate that not only could multiple AUVs of different types work together using a common on board autonomy structure, but that both research groups (the Massachusetts Institute of Technology's Laboratory for Autonomous Marine Sensing Systems from Cambridge, MA, USA, and the researchers and AUV team from NURC) could collaborate their efforts to advance the quality and quantity of data collected.

Acoustic communication is used nearly exclusively during our AUV operations for AUV-to-AUV and AUV-to-ship/lab (via gateway buoy or Towfish modem) scientific and navigational data exchange in virtually real-time (delays on the order of seconds to minutes). The software behind this is the Goby Underwater Autonomy Project through the pAcommsHandler interface for the Mission Oriented Operating Suite (MOOS) [14], [15] autonomy system. A common suite of autonomy software is used on board each AUV and the topside (operator) computers to tie together all of the pieces to allow the AUVs to collaborate autonomously with each other and adapt to the environment. Both the MIT and NURC groups use the MOOS and the IvP Helm (IvP stands for Interval Programming), which work in conjunction to make the AUVs carry out a variety of autonomy behaviors. These behaviors autonomously and adaptively reason over AUV heading, speed, and depth, depending on the behaviors that the operators set as active on each AUV [16], [17].

This paper will cover the goals of the Internal Wave Detection Experiment on 13 August, 2010, during the GLINT '10 filed trials in the Tyrrhenian Sea west of Italy, comparing it with similar experiments from other literature. This is followed by details of the experimental setup

and implementation from GLINT '10, including a discussion of the required instrumentation, communication, and autonomy systems. The resulting data sets from the AUV missions are then analyzed and compared with wave and buoyancy theory [2], [18] to determine the possible sources for dominant internal wave frequencies in the data. Finally, directions of future work are discussed and conclusions are drawn.

II. GOALS

The GLINT '10 Internal Wave Detection Experiment aimed to use multiple AUVs to detect the presence of internal waves (or lack thereof) in the region of the Tyrrhenian Sea bounded by the western coast of Italy and the islands of the Tuscan Archipelago (see Fig. 1).

Fig. 1. The region of the Tyrrhenian Sea bounded by the western coast of Italy and the islands of the Tuscan Archipelago. The Tuscan Archipelago basin is outlined by the dashed line. The GLINT '10 AUV operation region is delineated by the box. The numbering shows the five inlets of the basin.

The primary constraints were the necessity to have multiple AUVs collaborate their positions autonomously to execute the experiment and to make use of the ability to adapt AUV position to temperature changes in the environment. In these coastal Mediterranean waters ($\sim$ 110 m depth) with relatively constant salinity over depth, the water temperature dominates the density calculation in the equation of state for seawater [1]. This allows us to detect the presence of internal waves directly from the CT sensor's temperature measurements instead of needing to calculate density for each point in space. If successful, this experiment would be the first to use fully autonomously-collaborating AUVs that autonomously adapt their motion to changes

in the environment, thus efficiently capturing a synoptic data set that may contain internal wave signatures.

We also strove to successfully demonstrate the use of AUVs of different types, from different research groups, communicating and collaborating autonomously through MOOS and IvP Helm autonomy software and acoustically communicating using a predefined polling scheme that is set using the pAcommsHandler code.

III. Implementation

A. Hardware Platforms

To deploy the AUV missions (detailed below) for the Internal Wave Detection Experiment, we required two actively propelled AUVs and an acoustic communications 'gateway' buoy. In addition, we were able to attach 10 thermistors to the wet line on the buoy to create a thermistor chain. The AUV command and control center, or 'topside,' was located in the lab on the NRV Alliance, positioned within 5 km range from the deployed AUVs and buoy for the experiment's duration.

The Bluefin 21" AUV named Unicorn is operated by our group in the Laboratory for Autonomous Marine Sensing Systems at the Massachusetts Institute of Technology (MIT). It has a 21" hull diameter and was $\sim$3 m in length in the GLINT '10 experiment configuration shown in Fig. 2. Unicorn's speed range for best motion control is 1.0-1.8 m/s, though she is often commanded to travel at 1.5 m/s (although this varies if Unicorn is running according to autonomous adaptation behaviors) and has poor vertical stability below 1.3 m/s. Navigation instrumentation for Unicorn consists of a Leica DMC-SX Magnetic Compass and a Crossbow AHRS (attitude heading reference sensor) resulting in a navigational error of about $1\% - 5\%$ of the distance traveled between acquiring GPS position fixes. This navigational error assumes Unicorn has constant DVL (Doppler velocity log) bottom-lock, has completed a compass hard iron/soft iron calibration, has completed a compass star maneuver (for compass calibration in the water), and the Bluefin software on board has done some calibrations and math to improve the navigational accuracy to this point. As such, Unicorn must surface for a GPS position fix every 30 minutes, resulting in about 50-100 m of navigational error. Other instrumentation on Unicorn during GLINT '10 consisted of a CT sensor, a pressure sensor, and an acoustic modem with transducer.

Fig. 2. The Bluefin 21" Unicorn AUV operated by the MIT Laboratory for Autonomous Marine Sensing Systems. Used with permission from [19].

The Ocean Explorer (OEX) AUV named Harpo is operated by a group at the NATO Undersea Research Centre (NURC) based in La Spezia, Italy. It has a 21" hull diameter and was 4.3 m in length in the GLINT '10 experiment configuration shown in Fig. 3. Harpo's maximum speed is quoted at about 1.2 m/s, though it is often run slower to conserve battery power. For navigation, Harpo runs an IMU (inertial measurement unit) in conjunction with an acoustic DVL with bottom-lock that has little position drift (under 100 m) over the course of the day (often about 7 hours of runtime) after completing an in-water navigation alignment each morning [20]. This means that Harpo does not need to surface for GPS position fixes during experiments. Other instrumentation on Harpo during GLINT '10 consisted of a CTD sensor, and two acoustic modems with transducers.

Both AUVs were equipped with a WHOI WH-BT-2 28 kHz acoustic transducer [21] and on board payload computers running Linux operating systems with MOOS and IvP Helm autonomy software and the pAcommsHandler acoustic communication polling handler, similar to that used on the topside computers.

The MIT topside maintained radio frequency (RF) communication with the gateway buoy through a Freewave antenna mounted outside the upper deck of the NRV Alliance and acoustic communication with the AUVs via the acoustic modem transducer and hydrophone array hanging

Fig. 3. The NURC OEX-Harpo AUV used during GLINT '10. This AUV communicates with the ship and the MIT Unicorn AUV via acoustic communication (underwater). It also carries a GPS for positioning.

from the gateway buoy. The NURC topside maintained acoustic communication with Harpo via a Towfish acoustic modem transducer hanging in the water over the side of the ship. Both groups' topside computers included a Google Earth Ocean Viewer (GEOV) situational display of all AUVs, buoys, ships, and instruments in the water as in Fig. 4 [22], as well as the AUV command and control software (MOOS and IvP Helm) and pAcommsHandler acoustic message encoding/decoding and queuing/sending code.

The gateway buoy was a Micro-modem VSW Modem Buoy built by the Woods Hole Oceanographic Institution (WHOI) Acoustic Communications Group [21]. It was equipped with a GPS unit and Freewave RF antenna on the surface expression and a hanging wet cable of approximately 30 m length equipped with a 4-hydrophone array (for high-rate communication) and an acoustic modem transducer at the bottom. The buoy itself was stationed at the center of the AUV loiter patterns during each mission.

The 10 thermistors were placed along the buoy's wet cable at approximately 3 m spacing and sampled the temperature every 30 seconds as a ground-truth for the presence of internal waves in the region.

B. AUV Missions

This experiment initially consisted of three AUV missions, however only the first two were completed due to time constraints and operational difficulties. From an early morning ship CTD

cast and some pre- and mid-experiment yo-yos through the water column using Unicorn, the peak temperature change of the thermocline was noted at 10 $\pm$1 m depth throughout most of the day. Also note that performing horizontal loiter patterns on a radius of O(500 m) may be considered a point measurement relative to the scale of the large basin bounded by the Tuscan Archipelago, though on a local scale the pentagonal shape of the loiters (each of the 5 legs providing wave information from a different direction) has potential to enable us to determine the direction of travel of internal waves. A screen shot of the situational display from Mission 2 is shown in Fig. 4 to help visualize the mission layouts, and details of each mission are presented in Tables I, II, and III. Descriptions of the adaptive autonomy behaviors used follow in Section III-C.

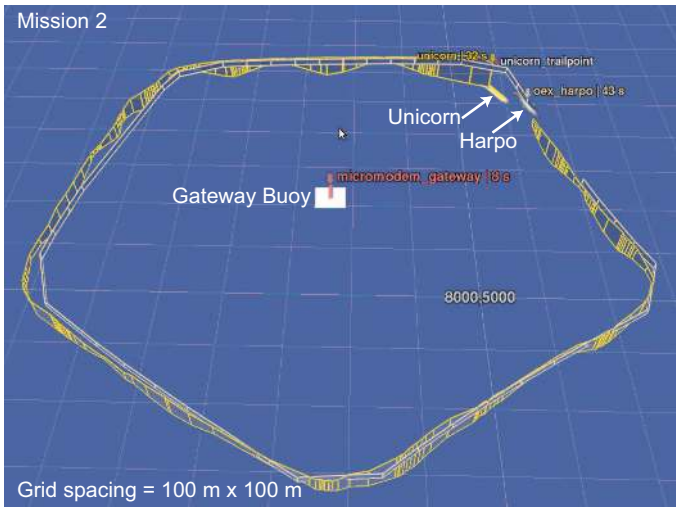

Fig. 4. Mission 2 loiter pattern around the gateway buoy, as seen from above, at an angle to the horizontal. Harpo performs a horizontal loiter pattern at constant depth (12 m) just below the thermocline. Unicorn trails directly behind Harpo while performing an adaptive yo-yo pattern through the thermocline depth range. Vertical bars along the loiter indicate the AUVs' depths (yellow is Unicorn's track, white is Harpo's track), and their current positions are shown by the arrows. Best viewed in color.

C. MOOS Processes and IvP Helm Autonomy Behaviors

As previously mentioned, MOOS is the underlying autonomy software on board the AUVs and on the topside operators' computers. MOOS is essentially a publish-subscribe architecture that passes messages between autonomy processes and behaviors on board each AUV, as well

TABLE I

MISSION 1

Description	60 m depth loiter & 10 m depth trail loiter
OEX-Harpo	
Horizontal pattern	pentagonal loiter, 550 m radius, clockwise travel
Depth	60 m, constant depth behavior
Speed	1.3 m/s
BF21-Unicorn	
Horizontal pattern	trail Harpo at 150 m range, 180° relative trail angle (directly behind Harpo)
Depth	at thermocline ∼10 m, adaptive constant depth behavior (changed to 12 m, constant depth behavior during experiment)
Speed	1.3 m/s (adaptive to trail Harpo)

as through the water between the AUVs and the topside computer [16]. The brains behind the autonomy lie in the IvP Helm (IvP stands for Interval Programming) code that is integrated into MOOS to implement the use of autonomy behaviors (e.g., vertical yo-yos, trail-an-AUV, horizontal racetracks, safety behaviors) on the AUVs. These behaviors optimize over an AUV's heading, speed, and depth to control its motion through the water, depending on what behavior is being followed [16], [17]. The MOOS processes and behaviors most relevant to the Internal Wave Detection Experiment are described below.

1) Environmental Gradient Determination Process: pEnvtGrad: One process that is run using MOOS is the environmental gradient determination process, pEnvtGrad, used to perform thermocline tracking and similar environmentally adaptive behaviors. This process monitors and sorts an AUV's CTD data, using the data to calculate vertical gradients of temperature ($|\partial T/\partial z|$) through the water column, the depth range (upper and lower bounds) covered by the thermocline, and the depth at which the thermocline gradient is strongest (maximum $|\partial T/\partial z|$). These calculated values are then published to the MOOS database on the AUV to be used to guide environmentally-focused adaptive behaviors, such as the adaptive yo-yo (toggle depth) behavior and the adaptive constant depth behavior described below. pEnvtGrad is run concurrently with

TABLE II

MISSION 2

Description	10 m depth loiter & adaptive yo-yo trail loiter (depth-adaptive to thermocline)
OEX-Harpo	
Horizontal pattern	pentagonal loiter, 550 m radius, clockwise travel
Depth	at thermocline $\sim$10 m, adaptive constant depth behavior (changed to 12 m, constant depth behavior during experiment)
Speed	1.3 m/s
BF21-Unicorn	
Horizontal pattern	trail Harpo at 150 m range, 180° relative trail angle (directly behind Harpo)
Depth	adaptive yo-yo (toggle depth) behavior within thermocline depth range (calculated by pEnvtGrad), beginning with 7-70 m dive range
Speed	1.3 m/s (adaptive to trail Harpo)

either of these depth-adaptive behaviors. The calculated values are also used by other MOOS processes and behaviors that need to know environmental information, and the thermocline boundary and peak gradient values are sent acoustically to other AUVs as informational data and to the topside for monitoring by the AUV operators. pEnvtGrad also calculates analogous values for profiles of sound speed and density, which are derived from temperature, salinity, and pressure measurements. A conceptual sketch of the adaptive thermocline tracking process using pEnvtGrad is shown in Fig. 5. The AUV performs an initial yo-yo dive from the surface to as deep as allowable while collecting temperature (and / or salinity and pressure) data. The water column is divided into many depth bins, over which temperature measurements are averaged, then the vertical gradients of temperature ($\partial T/\partial z$) are calculated between depth bins. The magnitude of the average of the vertical temperature gradients is set as the threshold value, and any depth bin in which $|\partial T/\partial z|$ exceeds the threshold value is flagged as being within the thermocline. Thus, we are able to define an upper and lower depth bound for the thermocline region and

TABLE III
MISSION 3

Description	concentric loiters at 10 m depth & depth-adaptive to thermocline (adaptive yo-yo), outer AUV trails (not completed)
OEX-Harpo	
Horizontal pattern	pentagonal loiter, 450 m radius, clockwise travel
Depth	at thermocline ∼10 m, adaptive constant depth behavior
Speed	1.0 m/s
BF21-Unicorn	
Horizontal pattern	trail Harpo at 150 m range, 315° relative trail angle (off Harpo's stern and to port, resulting in 550 m radius outer loiter)
Depth	adaptive yo-yo (toggle depth) behavior within thermocline depth range (calculated by pEnvtGrad), beginning with 7-70 m dive range
Speed	1.5 m/s (adaptive to trail Harpo)

define the peak thermocline depth as the depth bin with the maximum $|\partial T/\partial z|$. More detail on the algorithms used by pEnvtGrad and related field trials can be found in [23].

In our GLINT '10 Internal Wave Detection Experiment, pEnvtGrad was employed by unicorn in Mission 2 to obtain a three-dimensional data set of the temperature variations in the operational region, which will ultimately be used to analyze internal wave amplitudes.

2) Adaptive Yo-Yo (Toggle Depth) Behavior: The adaptive yo-yo (toggle depth) IvP Helm behavior, BHV_ToggleDepth, controls the desired depth of an AUV. It sets the desired upper and lower depth boundaries of a vertical yo-yo (or sawtooth) pattern for the AUV based on the upper and lower depth boundaries of the thermocline, as determined by pEnvtGrad (during the Internal Wave Detection Experiment). That is, as the thermocline boundary depths change over the course of a thermocline tracking mission (as in Mission 2), BHV_ToggleDepth adapts the boundaries of the AUV's yo-yo to match those of the thermocline in real-time by toggling the

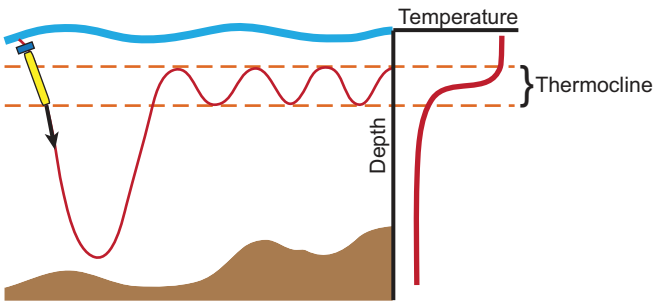

Fig. 5. A conceptual sketch of an AUV performing thermocline tracking using pEnvtGrad. The AUV completes a dive from the surface to as deep as allowable, collecting temperature data. The depth range of maximum temperature change per unit depth is determined as the thermocline region. The calculated upper and lower bounds of the thermocline region are then used to bound the vertical yo-yos of the AUV, essentially tracking the thermocline region. Used with permission from [23].

commanded depth between these two bounds to ensure that the desired depths are achieved. BHV_ToggleDepth can be active while performing any horizontal deployment pattern (e.g., racetrack, loiter, zig-zag, track-and-trail).

3) Adaptive Constant Depth Behavior: The adaptive constant depth IvP Helm behavior uses BHV_ConstantDepth to set a single desired depth for an AUV to swim at based on the peak thermocline depth (the depth of maximum temperature change per unit depth) calculated by pEnvtGrad. As the peak thermocline depth shifts up or down in the water column, the desired AUV depth commanded by BHV_ConstantDepth is automatically updated to match it, autonomously adapting to the changes in the environment in real time. Unfortunately, swimming an AUV at the peak thermocline depth results in very poor acoustic communications to and from that AUV, so we opted to command the AUVs to a constant depth a couple of meters below the peak of the thermocline with the non-adaptive mode of BHV_ConstantDepth such that we could continue to monitor the AUVs regularly throughout the missions and so that the AUVs could communicate with each other to perform the track-and-trail behavior.

4) Track-and-Trail Mode: The track-and-trail mode puts the trailing AUV into 'TRAIL' mode, shadowing a leading AUV (or any leading platform for which the trailing AUV receives position updates via acoustic messages) in the horizontal plane. The relative bearing and trailing distance from the trailing AUV to the leading AUV must be set by the operator, and the depth modes (e.g., constant depth, adaptive constant depth, adaptive yo-yo toggle depth) of the two AUVs are

set independently of each other and independently of being in TRAIL mode. The leading AUV is not in TRAIL mode (unless it is trailing yet another platform) and leads the mission in the horizontal plane.

5) pAcommsHandler: The Goby Underwater Autonomy Project's MOOS interface, pAcommsHandler, controls the queuing and sending of data through the underwater acoustic channel on all acoustically-communicating platforms we use and is crucial to all of our AUV missions. It encodes the data (science data, navigation data, status data, etc.) on one node (AUV, topside, or gateway buoy), slots the encoded message into the polling queue, initializes the acoustic transmission, and decodes the data when they are received on another node running pAcommsHandler [14], [15]. This all occurs while missions are underway on the AUVs, resulting in virtually real-time data transmission. This real-time communication is necessary when there are multiple AUVs in the water that need to know information about one another to collaborate their motions and avoid collisions. Finally, it is also important to the topside operators, who want real-time data updates to monitor the progress and autonomy behaviors of the AUVs and to monitor the changes in their environment and scientific data over the course of an AUV mission.

IV. Results

This section compiles not only results of the data processing to determine the internal wave frequencies and whence they originated, but also some of the unexpected effects that the field deployment had on the planned missions and resulting data. These effects are largely due to physical constraints of the AUVs and instruments and imposed effects of a dynamic ocean environment on conducting AUV missions. A brief description of the oceanographic conditions on the day of the experiment is presented first.

A. Oceanographic Conditions

Fig. 6 shows the morning and afternoon sound speed, temperature, salinity, and density profiles from a CTD cast from the NRV Alliance on 13 August, 2010, in the GLINT '10 operation area. The water depth at the CTD sample locations (and much of the operation area) was just over 110 m. Here we see a warm isothermal mixed layer near the surface of approximately 10 m depth and 24 °C resulting in a strong thermocline at about 10 m depth. The temperature then drops suddenly with depth to about 19 °C, then tapers off to about 14 °C by 60 m depth,

below which the water remains isothermal. The steep thermocline near 10 m depth suggests that internal waves would be most prominently observable at that depth, if they exist. It should be noted that the high frequency variations in salinity over depth are likely due to the sensitivity of the conductivity sensor on the CTD to the rapid changes in temperature between 9 and 60 m. Sound speed was calculated using the Mackenzie sound speed equation [24]. Density was calculated from the Unesco 1983 equation of state for sea water [1].

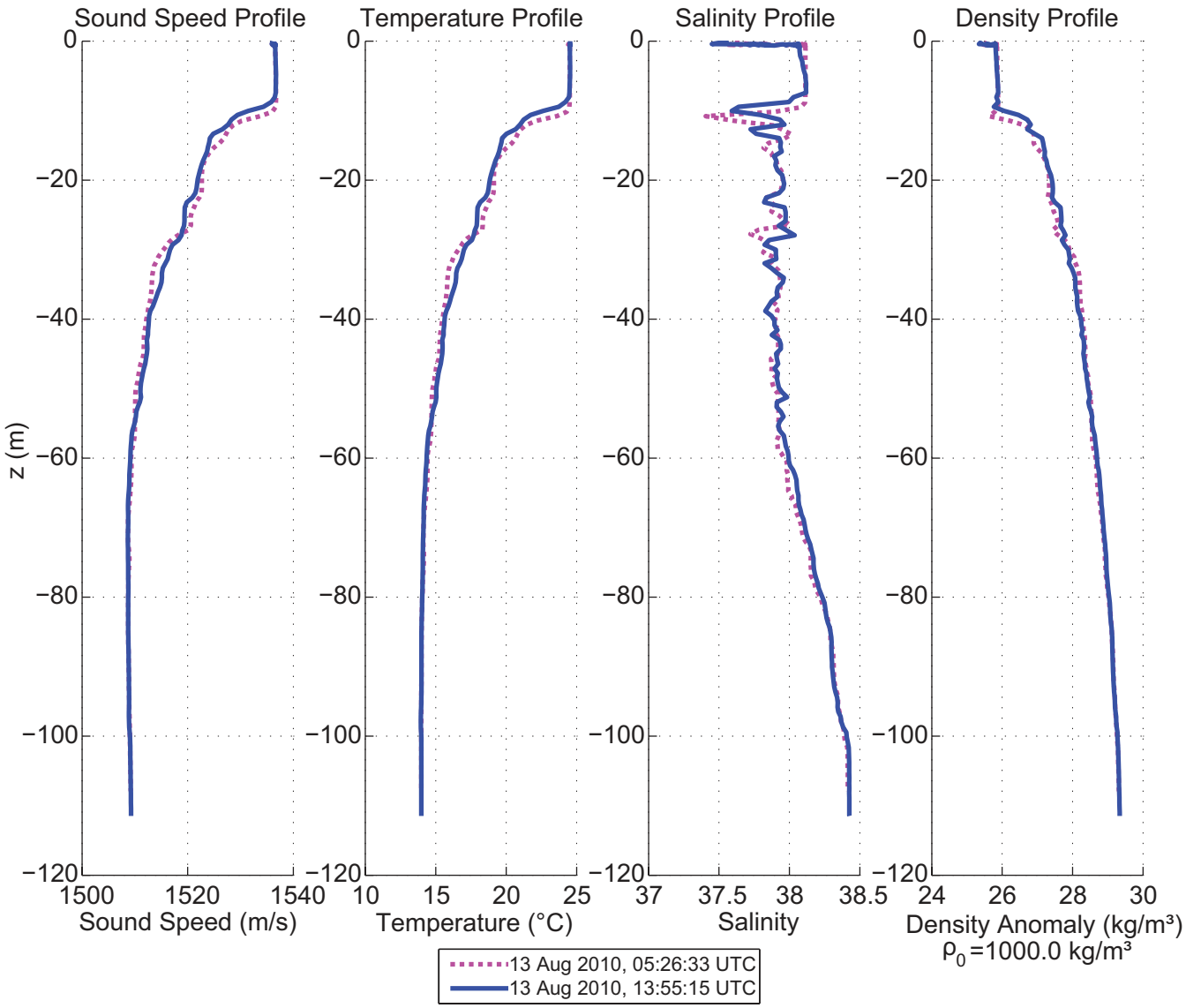

Fig. 6. Morning and afternoon sound speed, temperature, salinity, and density profiles from a CTD cast from the NRV Alliance on 13 August, 2010.

B. Mission Execution

At the beginning of the Internal Wave Detection missions, we commanded the shallow-depth AUV to swim at the depth of the maximum gradient of the thermocline ($\sim$ 10 m depth). This resulted in extremely poor acoustic communication observed between the shallow AUV (Unicorn, for the first mission) and the topside (via the gateway buoy) due to the fluctuating refraction direction of propagating sound waves in the steepest region of the thermocline (depth of maximum $|\partial T/\partial z|$). With Unicorn traveling at 10 m depth, 3/14 (21%) of the acoustic messages sent by Unicorn to the topside were received on the topside, while 19/38 (50%) of them were received on the topside with Unicorn traveling at 12 m depth (acoustic communication performance values based on rate 0 FH-FSK (frequency-hopped frequency shift keying) messages sent from Unicorn to the gateway buoy, data courtesy of Toby Schneider, MIT). Subsequent missions had the depth of the shallow (constant depth) AUV changed to swim at 12 m –just below the peak gradient of the thermocline– from the start of the mission to avoid losing contact with that AUV.

The next challenge faced during deployment was a difference in speed ranges achievable by Unicorn and Harpo. This was significant because, in order for Unicorn to trail behind Harpo without overtaking Harpo, Unicorn had to slow to its minimum speed of 1.3 m/s while Harpo had to travel at 1.3 m/s, just above Harpo's maximum quoted speed. When Unicorn slowed below 1.3 m/s to remain at a safe distance behind Harpo, its depth control degraded and it was observed to fluctuate involuntarily, or 'porpoise,' in depth by up to $\pm$0.8 m in a periodic manner, adding a detectable temperature fluctuation to its data set. Upon processing, the power spectral density peaks at the dominant frequencies of Unicorn's porpoising were subtracted from the temperature spectrum ($PSD_{Temp_pure} = PSD_{Temp_Unicorn} - PSD_{Depth_Unicorn}$) to minimize their influence on the results. During Mission 2, Unicorn's minimum speed was not a problem because it was slowed in horizontal speed by the yo-yo depth excursions it was performing.

During the second mission in which Unicorn was adapting its yo-yo depth range to focus around the thermocline, hysteresis was observed in the temperature data (see Fig. 7). As Unicorn ascended through the 12-meter depth mark, the temperature was consistently observed to be lower than the AUV's subsequent descent through the 12-meter depth mark. In Unicorn, the CT sensor is mounted mid-way between the nose and tail of the AUV, and the pressure sensor (giving

depth readings) is mounted in the aft section of the AUV. Thus, if there were any appreciable lag between sensor readings of temperature and pressure at 12 m, the temperature reading at 12 m would be expected to be higher on the ascent (CT sensor at the mid-section is higher in the water column than the aft pressure sensor) and lower on the descent, which is the opposite of what has been observed. The Sea-Bird Electronics, Inc., model SBE 37-SI CT sensor on Unicorn has an acquisition time of 1.0-2.6 seconds/sample [25], which is comparable to the $\sim$1.5 s it takes the pressure sensor to catch up in depth to where the previous temperature measurement was taken, which may account for some of the discrepancy, and thus, the hysteresis. The resolution of the temperature sensor on Unicorn is specified as 0.0001 °C [25], while depth sensor resolution is approximated at 0.5 m or less, based on observation. Thus, this temperature fluctuation is not due to the resolution of the temperature sensor, and we cannot conclude causation from the approximated resolution of the depth sensor. This leaves the only probable explanation of the temperature fluctuation as hysteresis between the CT and pressure sensors due to the slow acquisition time of the temperature sensor. One way to adjust for this in post-processing is to find the average temperature difference between each instance of shoaling and diving through the 12-meter depth mark, and add (subtract) half the difference to (from) the temperature measurement on the ascent (descent).

The thermistor chain was deployed throughout both successful AUV missions, however it was only sampling at a 30-second interval compared to the approximately 10 Hz and 4 Hz sampling frequencies of Unicorn and Harpo, respectively. This means that the thermistor data spectra are resolved for a much lower frequency range than the spectra from the AUVs' data (see Figs. 10, 12, and 14), allowing us to detect any possible lower-frequency internal waves.

Finally, atmospheric weather conditions can also affect underwater measurements through surface interactions of wind and waves. From approximately 0900-0930 UTC, or 1100-1130 local time ($\sim$30-60 min into Mission 1), a storm system passed over the ship and AUV operation area. Storms frequently sustain higher winds than clear-weather conditions, and introduce an influx of fresh water to the otherwise salty sea surface. Depending on the severity of the storm, its effects on the underwater environment may lag the storm and persist from hours to weeks after the storm has passed. In this case, the storm only covered a local area of about 200 km^2 with squalls of very heavy rain, and it did not appear to cause an appreciable change in the temperature at the thermocline immediately following the storm's passing. Over the course of

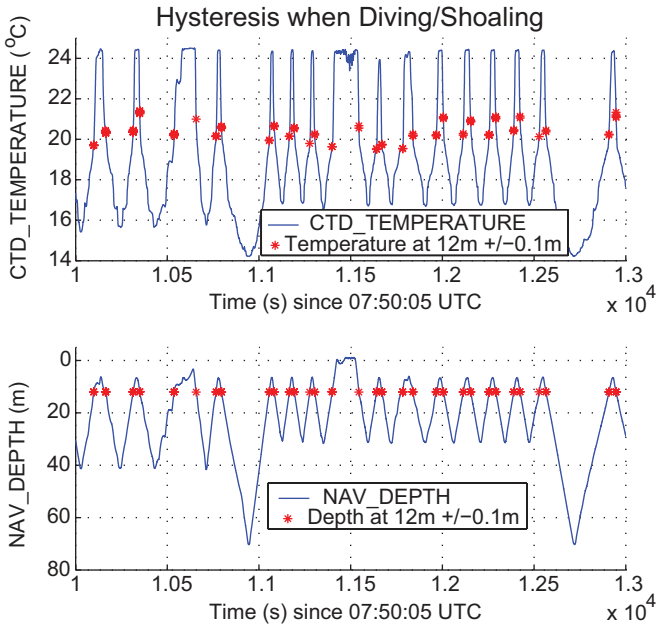

Fig. 7. Hysteresis is seen in Unicorn's temperature data (CTD_TEMPERATURE) while preforming yo-yos through the water column. NAV_Z values are the negative of Unicorns measured depth values. The stars signify temperature and depth measurements taken when Unicorn is at 12 ± 0.1 m depth. It has been verified that the ± 0.1 m depth range allowed is not the cause of the hysteresis.

the the entire day (end of Mission 1 and through Mission 2, about 4.5 hours), however, there was an overall decrease in temperature of $\sim$0.5 °C by the end of Mission 2. It is unlikely that this temperature decrease is due to the storm, since a deluge of 10 cm of water at 14 °C advected into the surface mixed layer (10 m deep, 24 °C) over the storm's area would only decrease the mixed-layer temperature by about 0.1 °C or less. Thus, it is more likely that this drop in mixed-layer temperature is due to surface cooling as the post-storm sunshine waned going into the mid-afternoon (local time).

C. Data Analysis

Since the goal of the Internal Wave Detection Experiment was to detect the presence of internal waves in the basin of the Tyrrhenian Sea bounded by the Tuscan Archipelago (or more specifically bounded by our small GLINT '10 operational area), we approached the data analysis from a signal processing standpoint once a baseline for temperature fluctuations was established. In order

to preserve any transient frequency peaks in the temperature spectra that may be representative of soliton internal waves, no data windowing was done to generate the Power Spectral Density (PSD) plots in this section.

1) Mission 1: Mission 1 lasted from 0833-0853 UTC with Unicorn at 10 m, and from 0913-1007 UTC with Unicorn at 12 m. Between these times, Unicorn was at 13 m, but for now we have set that short data set aside in favor of focusing on the times spans in which Unicorn was closest to the thermocline depth. Harpo was at 60 m from 0818-1120 UTC.

From Mission 1, Harpo's temperature data at 60 m depth (significantly below the thermocline region) exhibited a baseline of small fluctuations in temperature (± 0.3°C) as seen in Fig. 8. There is insufficient data, given the temporal sparsity of temperature profiles passing through 60 m depth and the small temperature change per unit depth at 60 m, to determine whether variations in these temperature data are due to internal waves or not.

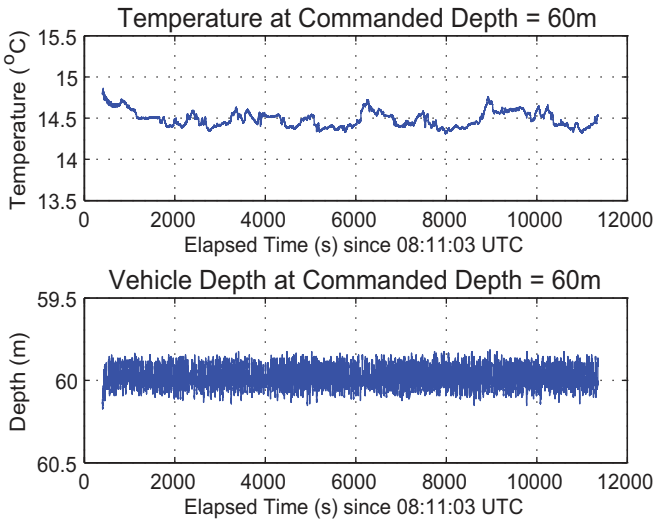

Fig. 8. Temperature and depth times series of data from Harpo at 60 m depth during Mission 1. This is used as a baseline measurement of the temperature fluctuations in the relatively density-homogeneous layer well below the thermocline.

In contrast, Unicorn's temperature data at 10 m and 12 m during Mission 1 revealed a number of peak-energy frequencies above the noise floor in its PSD plots (Fig. 9). Due to the porpoising motion of Unicorn during Mission 1, the PSD of Unicorn's depth was subtracted from the PSDs of temperature to get the 'pure' temperature spectra at 10 and 12 m ($PSD_{Temp\_pure} = PSD_{Temp\_Unicorn} - PSD_{Depth\_Unicorn}$). The frequencies and PSDs of the pure

temperature spectrum's local maxima at 10 m and 12 m depth are plotted as stars in Fig. 9. This is a satisfactory approach, since the lack of windowing captures frequencies of internal wave packets or solitons that traverse the operational region on a time scale significantly shorter than our overall mission length. To show the time variation of the spectra, we have also analyzed the temperature measurements at 10 m and 12 m using the spectrogram shown in Fig. 10. The broadband blips in energy at 30-minute intervals are a result of Unicorn surfacing at those times to acquire a GPS position fix. There appears to be a very weak but persistent narrow-band peak around 4.0 Hz in the 12 m spectrogram, which is well above the possible internal wave frequencies and probably due to sensor noise. Other potentially interesting peaks appear below 0.3 Hz at about 650-1150 s in the 10 m spectrogram and at about 700-800, 1250, 1700-1800, 2000-2500, 2550-2650, and 2950-3000 s in the 12 m spectrogram, some of which may belong to internal soliton waves. None of Unicorn's low-frequency (<0.05 Hz) energy peaks in the spectrogram are well distinguished from one time point to the next, thus we have chosen to leave out a low-frequency zoomed-in version of this plot.

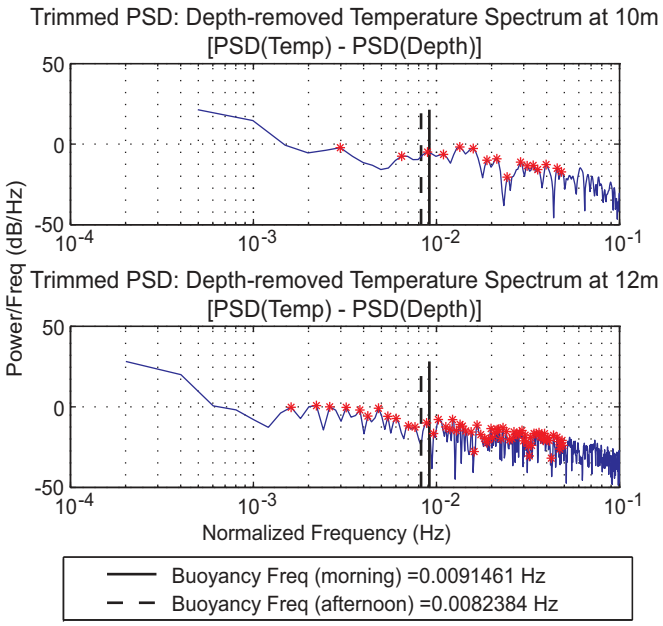

Fig. 9. Power Spectral Density plot from Unicorn's temperature data (depth variations removed) while traveling at 10 m (top plot) and 12 m (bottom plot) depth. Red stars correspond to local peak frequencies in the data spectra.

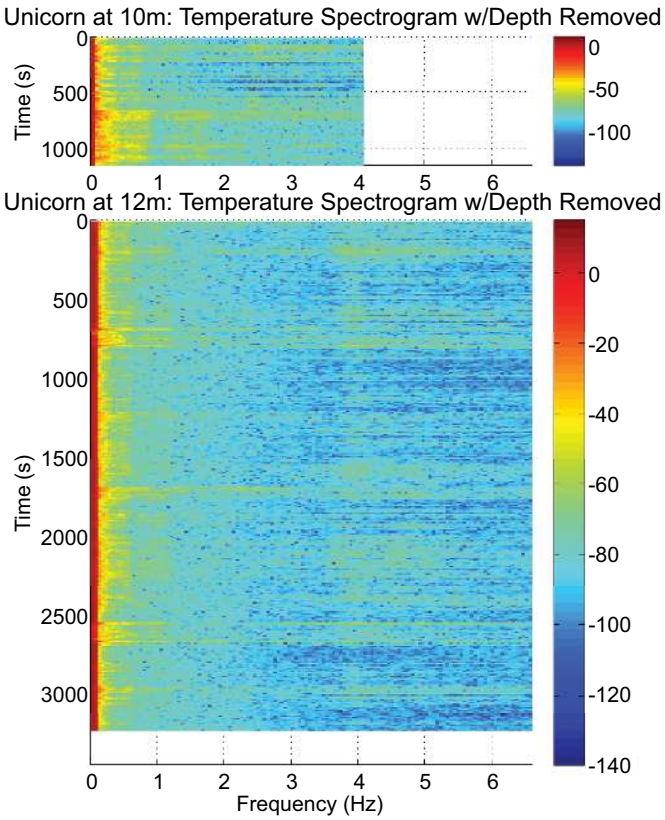

Fig. 10. Spectrogram of Unicorn's temperature data (depth variations removed) while swimming at 10 m (top plot) and 12 m (bottom plot) depth. Hamming window length: 256 samples. Color axis units: dB.

2) Mission 2: Mission 2 lasted from 1139-1250 UTC with Harpo at 12 m, though Unicorn tracked the thermocline adaptively from 1009-1327 UTC.

With a below-thermocline baseline data set established at 60 m during Mission 1, Harpo was re-tasked to swim at 12 m depth for Mission 2 to track just below the peak thermocline gradient as Unicorn did in Mission 1. Unicorn was re-tasked to perform adaptive thermocline tracking while autonomously trailing Harpo. Due to temporal separation of Missions 1 and 2, Harpo captured the passing of internal waves in its temperature data at 12 m which exhibited somewhat different peak frequencies than captured by Unicorn in Mission 1. A plot of Harpo's pure temperature spectrum at 12 m is shown in Fig. 11 with the peak PSD frequencies plotted as red stars. To show the time variation of the spectra, we analyzed the temperature measurements

at 12 m in the form of the spectrogram shown in Fig. 12. Harpo did not need to surface for GPS position fixes, so there are no broadband peaks at 30-minute intervals like the ones seen for Unicorn in Fig. 10. There again appears to be a very weak but persistent narrow-band peak, only this time it is around 1.7 Hz (beyond the axes of this plot, to highlight distinct lower-frequency peaks). Again, this peak is probably due to sensor noise. Other potentially interesting peaks appear below 0.015 Hz at about 500, 1300, 1800, 1900, 2200-2400, 2600, 3100, 4500, 5100, 5600, 6300, and 7400 s, some of which may belong to internal soliton waves.

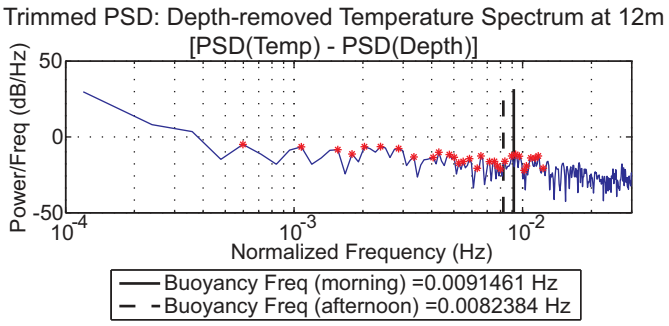

Fig. 11. Power Spectral Density plot from Harpo's temperature data (depth variations removed) while traveling at 12 m depth. Red stars correspond to local peak frequencies in the data spectrum.

3) Thermistor chain: A set of ten thermistors was deployed attached to the wet cable of the gateway buoy, positioned at the center of the AUV loiter pattern. The thermistors were at depths of 5, 8, 11, 14, 17, 21, 24, 27, and 30 m, with the tenth thermistor placed 0.5 m above the modem transducer. Since the precise depth of the tenth thermistor was not recorded, and the data set is similar to that of the 30 m thermistor only flatter (more isothermal) and about 2°C cooler, we have chosen to ignore this thermistor in our analysis. The thermistor chain began recording at 0600 UTC with a sampling frequency of 1/30 Hz, and continued to record the temperature through its recovery at about 1415 UTC. The temperature data for the upper 9 thermistors are shown in Fig. 13, ordered from shallowest (top) to deepest (bottom), plotted over time. Fluctuations in temperature are most prominently observed in the data from the thermistor at 11 m depth (closest thermistor to the thermocline depth), which may be indicative of internal waves propagating along the thermocline.

The spectrogram of the 11 m thermistor's temperature was plotted over varying time spans

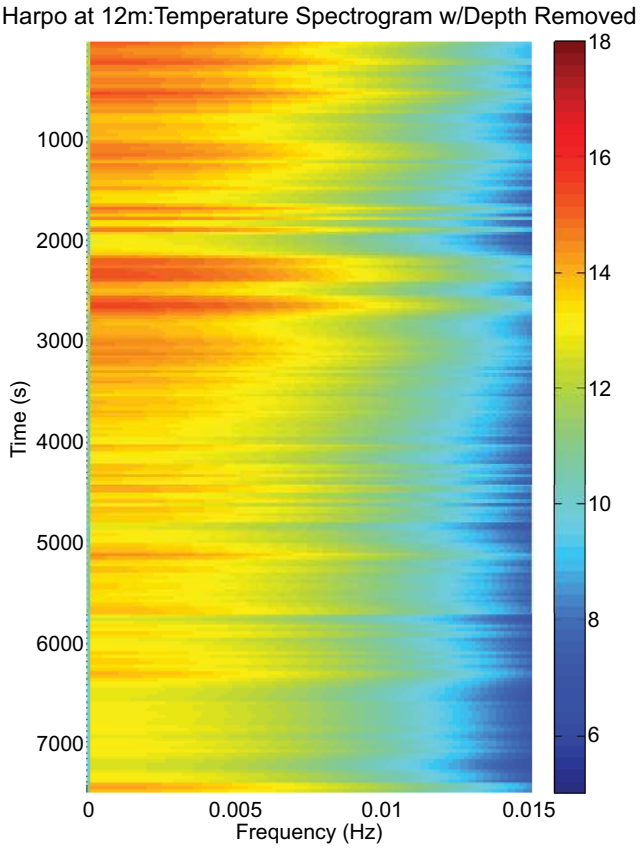

Fig. 12. Spectrogram of Harpo's temperature data (depth variations removed) while swimming at 12 m depth. Hamming window length: 256 samples. Color axis units: dB.

corresponding to when Unicorn was swimming at 10 and 12 m depth and when Harpo was swimming at 12 m depth (Fig. 14). These were visually compared to the spectrograms of the AUV-collected temperature data, and there is general qualitative agreement in times indicating low-frequency peaks, despite differing temporal resolutions. This range of temporal resolutions is due to the difference in sampling frequencies between the AUVs (about 4 Hz for Harpo and 10 Hz for Unicorn) and the thermistors (1/30 Hz).

The PSD plots of the temperature data for the 11 m thermistor are shown in Fig. 15, with the peak PSD frequencies plotted as red stars. Here we see dominant internal wave frequencies between 10^{-3} and 10^{-2} Hz (periods of 17 – 1.7 min) in all of the spectra that are similar to peaks in the AUVs' temperature spectra, while the full-length thermistor spectrum (top plot)

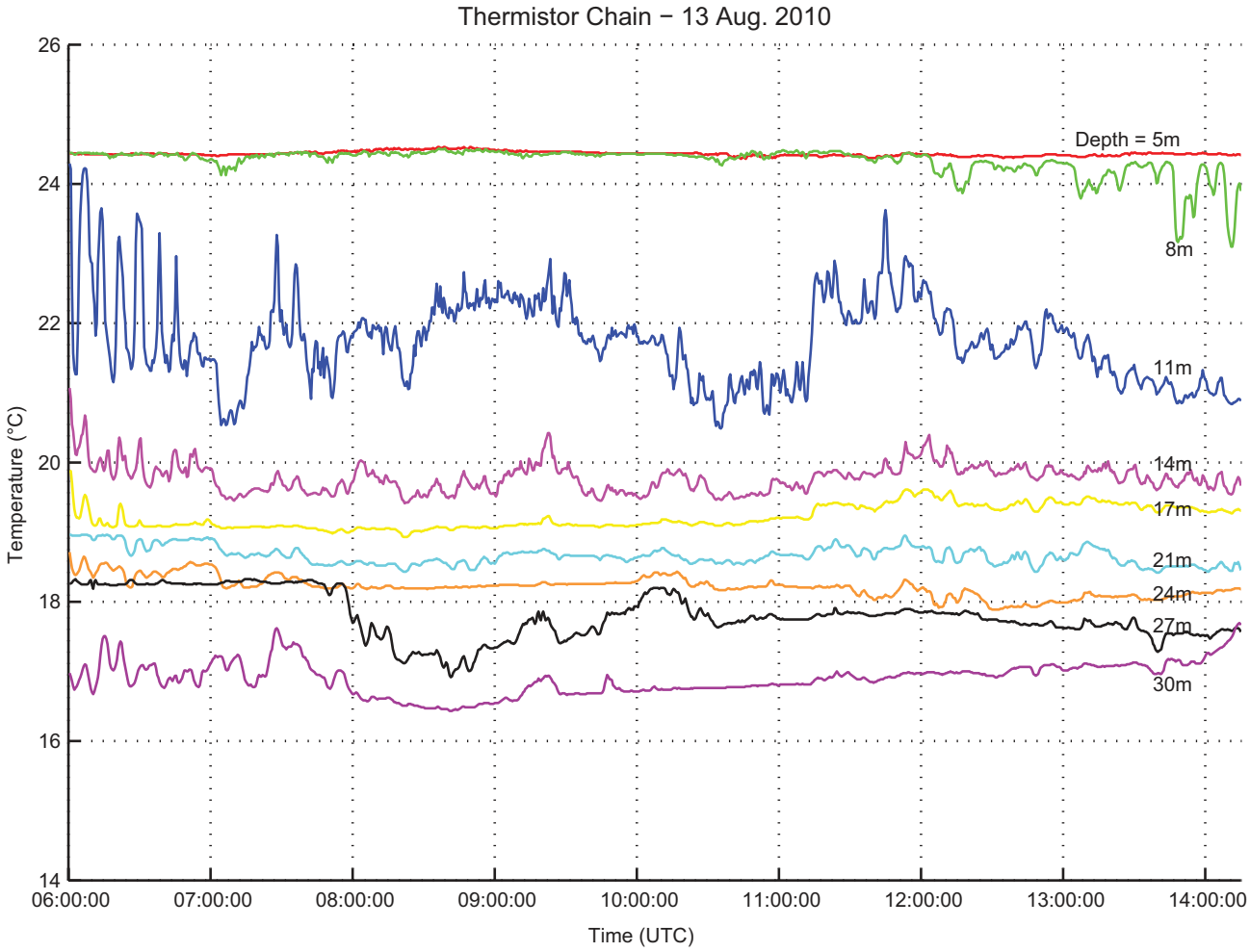

Fig. 13. Time series of temperature from the upper 9 out of 10 thermistors on the thermistor chain (the deepest thermistor is not shown since its precise depth was unknown). Increased temperature fluctuations are evident at the 11 m deep thermistor, closest to the 10 m thermocline depth.

also shows low-frequency peaks in the 10^{-4} – 10^{-3} Hz range (periods of 170 – 17 min). The time-windowed thermistor spectra corresponding to times the AUVs were at 10 and 12 m all have dominant frequencies of approximately 2×10^{-3}, 3×10^{-3}, and 6×10^{-3} Hz (periods of about 8, 6, and 3 min), strongly indicative of internal waves.

4) Buoyancy frequency analysis: We first decided to look at buoyancy frequency analysis with the dispersion relation (Equation 1) to solve for internal wave wavelength. Buoyancy frequency analysis states that the density difference over the thermocline interface supports its

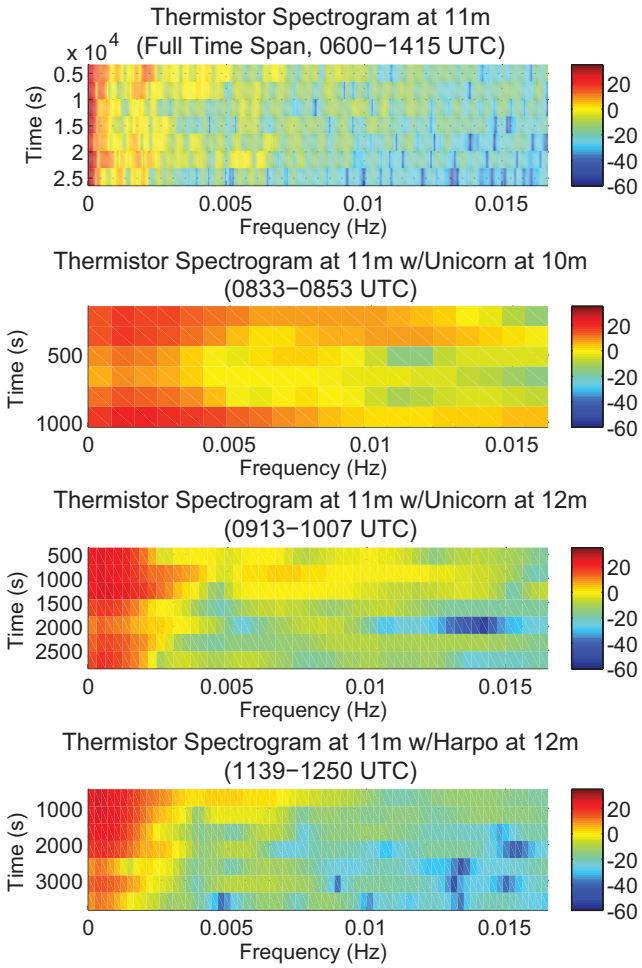

Fig. 14. Spectrograms of the temperature data from the thermistor at 11 m. From top to bottom: spectrogram of the full time span while the thermistor chain was in the water (Missions 1 and 2), the time span while Unicorn was at 10 m (Mission 1), the time span while Unicorn was at 12 m (Mission 1), and the time span while Harpo was at 12 m (Mission 2). No windowing. Color axis units: dB.

own 'buoyancy' frequency at which the interface is most likely to sustain internal waves [2]. Equation 1 approximates the baroclinic or internal mode of the vertical profile of the Tuscan Archipelago basin as a finite layer overlying an infinitely deep layer, with a density discontinuity (thermocline / pycnocline) at the interface between the two layers, giving

$$\omega^2 = \frac{g\ k\ (\rho - \rho_0) sinh(k\ h)}{\rho\ cosh(k\ h) + \rho_0\ sinh(k\ h)}, \tag{1}$$

where ω is the angular frequency in radians/s, g is 9.81 m/s^2 (gravitational acceleration),

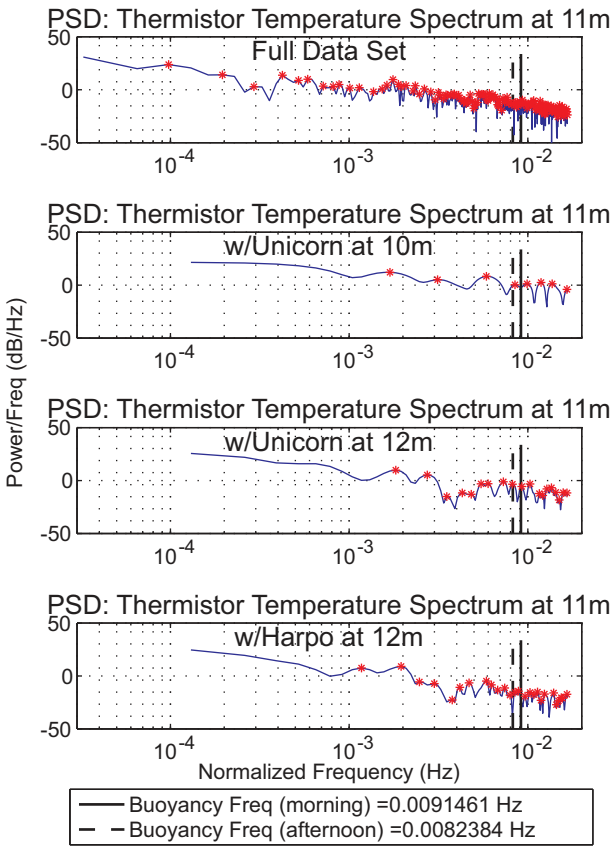

Fig. 15. PSDs of the temperature data from the thermistor at 11 m. From top to bottom: spectrogram of the full time span while the thermistor chain was in the water (Missions 1 and 2), the time span while Unicorn was at 10 m (Mission 1), the time span while Unicorn was at 12 m (Mission 1), and the time span while Harpo was at 12 m (Mission 2). Red stars are peaks in the spectra.

ρ_0 is the density above the pycnocline, $\rho = \rho_0 + \rho'$ is the density below the pycnocline, k is the wavenumber in radians/m, and h is the pycnocline depth in m ($\sim$11 m, experimentally determined). This form of the dispersion relation also assumes a that there is a free surface, which gives rise to a barotropic or surface mode that is beyond the scope of this paper. See [18] for more details on this form of the dispersion relation.

Given the temperature and density profiles taken the day of the experiment (Fig. 6), we approximate the thermocline and pycnocline depths as equal and use these terms interchangeably in this section. Starting from Equation 2 (the vertical component of the linearized Boussinesq equations for an inviscid liquid), we can define the Brunt-Väisälä frequency, or buoyancy frequency, N as

in Equation 3,

$$\frac{\partial^2 \eta}{\partial t^2} = \frac{g}{\rho}\frac{\partial \rho_0}{\partial z}\eta \tag{2}$$

$$N = \left(-\frac{g}{\rho}\frac{\partial \rho_0}{\partial z}\right)^{1/2} \tag{3}$$

where η is the amplitude of the internal wave, $\rho = \rho_0 + \rho'$ is the density of the fluid layer below the thermocline, and N $(= \omega)$ is an angular frequency of simple harmonic motion. Further details on the physics behind this buoyancy analysis can be found in [2], [18].

Using the Unesco 1983 equation of state for sea water [1], density was calculated based on the temperature, salinity, and pressure data collected across 12 m depth over the course of the field experiment. From the density and depth data, we estimate the partial derivative in Equation 3 as a finite difference over the pycnocline depth for both the morning and afternoon density profiles and solve for the bounding values of $N_{morning} = 0.05747$ rad/s (linear frequency of $f_{morning} = 0.009146$ Hz, period of $T_{morning} = 109.34$ sec) and $N_{afternoon} = 0.05176$ rad/s (linear frequency of $f_{afternoon} = 0.008238$ Hz, period of $T_{afternoon} = 121.38$ sec). Since the CTD cast data that these values are calculated from occurred just before and after the Internal Wave Detection Experiment in 13 August, 2010, we can take the calculated buoyancy frequency values as the upper and lower bounds for that day. The morning and afternoon linear buoyancy frequencies are plotted on the PSD plots in Fig. 9, 11, and 15. According to Kundu and Cohen [18], internal gravity waves are only sustainable below the buoyancy frequency along the interface (pycnocline). Thus, we will disregard all peak frequencies detected above $f_{morning} = 0.009146$ Hz. It is evident that there are a number of small peaks near and just below the buoyancy frequency in the AUV and thermistor PSD plots, strongly suggesting that buoyancy-supported internal waves propagated through the operation region during the experiment.

We can now use the dispersion relation, Equation 1, (with $\omega = N$, $h_{morning} = 11.79$ m, and $h_{afternoon} = 10.39$ m) to solve for k. Solutions for wavelength (λ) and wave phase speed $(c_p = \lambda f)$ follow naturally from Equations 4 and 5.

$$\lambda = \frac{2\pi}{k} \tag{4}$$

TABLE IV

EXPECTED INTERNAL WAVE VALUES CALCULATED USING THE BUOYANCY FREQUENCY

Time (UTC)	N (rad/s)	f (Hz)	T (s)	h (m)	k (rad/m)	c_p (m/s)	λ (m)
05:26:33	0.05747	0.009146	109.34	11.79	0.6169	0.09315	10.18
13:55:15	0.05176	0.008238	121.38	10.39	0.6161	0.08402	10.20

$$k = \frac{\omega}{c_p} \tag{5}$$

Using a graphical solution method due to the nonlinear nature of the dispersion relation, we estimated the values for k, λ, and c_p of internal waves as summarized in Table IV. In shallow water, the dispersion relation may often be simplified further by saying that any waves supported on the interface between two fluids of different density will have wavelengths much longer than the average water depth, $H = 150 - 200$ m (i.e., $\lambda \gg H$). However, we cannot assume the shallow-water (long-wave) approximation here since λ is actually less than the water depth by an order of magnitude (and on the order of the pycnocline depth), based on the unsimplified dispersion relation in Equation 1.

With the maximum phase speed, c_p, of the buoyancy-driven internal waves calculated to be 0.09315 m/s, the temperature sensors on both Unicorn and Harpo (and the thermistor chain) had ample time ($\sim$3 hrs per wave) to gather enough data to resolve the internal wave motion through the 1.1 km diameter of the loiter. In the case of Mission 1, Unicorn was at 10 m for 20 min and at 12 m for 54 min, and for Mission 2, Harpo was at 12 m for 71 minutes.

Given the very good agreement between the theoretical and data-derived peak wave frequencies (from both the AUVs' and the thermistor data), along with the slow $\sim$9 cm/s phase speed and $\sim$10 m wavelength of predicted internal waves near the thermocline depth (10–12 m), it is reasonable to conclude that internal waves were positively detected near and below the theoretical buoyancy frequency along the thermocline in the AUV operation region on 13 August, 2010, with most frequency components in the 10^{-3} – 10^{-2} Hz range.

5) Helmholtz-like 'Basin resonance' analysis: Another possible source of internal waves at the depth of the thermocline may be the Tuscan Archipelago basin acting as a Helmholtz resonator

due to flow through the inlets to the basin that lead out to the larger Northern Tyrrhenian Basin (see Fig. 1). The canonical example of Helmholtz resonance is the acoustic tone produced by blowing air across the neck of a bottle. The difference in our case is that the restoring force is hydrostatic pressure rather than compressed air, so we will call this 'Basin resonance'. As water depth fluctuates with water flowing into and out of the basin, it is possible that a low-frequency wave mode is excited along the thermocline as well. The openings, or inlets, where the forcing of water (and highest flow velocities) into and out of the basin may occur are the numbered segments in Fig. 1. The basin inlets are modeled as resonating masses, and the basin body is approximated to be at rest. Equations 6 and 7 describe this motion,

$$m_{inlet}\ddot{x} + \Delta P A_{inlet} = 0 \tag{6}$$

$$\Delta P = \frac{\rho g A_{inlet} x}{A_{surf}} \tag{7}$$

where m_{inlet} is the mass of an inlet, A_{inlet} is the cross-sectional area of an inlet, ΔP is the pressure change due to the basin changing depth, A_{surf} is the surface area of the basin, $g = 9.81$ m/s^2 is the gravitational acceleration, and ρ is the average water density. This is analogous to a simple harmonic oscillator described by the differential equation

$$m\ddot{x} + kx = 0, \tag{8}$$

where $k = k_{eff}$ is the effective spring constant of the basin given by

$$k_{eff} = \frac{\rho g A_{inlet}^2}{A_{surf}}. \tag{9}$$

The natural (resonant) frequency of a harmonic oscillator is $\omega_0^2 = k/m$. Thus we expect the basin to resonate at

$$\omega_0 = \left(\frac{g A_{inlet}}{A_{surf} L_{inlet}} \right)^{1/2}, \tag{10}$$

where L_{inlet} is the length of an inlet. To detect the contributions of different combinations of the five inlets, we average the ratios, A_{inlet}/L_{inlet}, of the inlet cross-sectional area to inlet

TABLE V
INLET DIMENSIONS CORRESPONDING TO INLETS IN FIG. 1, ESTIMATED USING GOOGLE EARTH [26]

Inlet	Width (m)	Depth (m)	Area, A (m^2)	Length, L (m)
1	7933	10	79330	4309
2	12635	40	505400	2710
3	28944	120	3473280	4700
4	42670	450	19201500	6000
5	13700	80	1096000	9350

length over the selected inlets as in Equation 11, where the subscript $j \in \{1, 2, 3, 4, 5\}$ (some combination of any of the 5 inlets).

$$\omega_0 = \left(\frac{g}{A_{surf}} \left(\frac{A_{inlet_j}}{L_{inlet_j}} \right)_{avg} \right)^{1/2} \tag{11}$$

If we estimate that the basin covers an area of $A_{surf} = 3880$ km^2 (estimated using Google Earth [26] in conjunction with a number of Internet-based area calculator tools for KML files) and the the inlet dimensions are as given in Table V, we calculate the resulting Basin frequencies $f_{Basin} = \omega_0/2\pi$.

Fig. 16 summarizes the Basin resonance frequencies compared to the low-frequency peaks in the AUVs' and thermistor's temperature data near the thermocline. Looking at the internal wave frequencies derived from the Unicorn and Harpo data, no evidence of Basin resonance can be seen in the waves along the thermocline. This is not surprising, given that the AUV missions ranged from 20 to 71 minutes in duration, which were barely long enough to span most of the possible Basin resonance periods due to certain inlets. When compared to the frequencies in the 11 m thermistor data (covering over 8 hours), however, there are a number of low-frequency peaks in the vicinity of the Basin resonances. Thus, it is very likely that we are seeing some evidence of Basin resonance in the thermistor's temperature spectrum at 11 m depth.

It is important to note that the calculated Basin frequencies in Fig. 16 may shift depending on the estimate of the basin surface area. Thus, the thermistor markers tend to align with different, but neighboring, Basin frequencies if the surface area is estimated differently. With an estimated

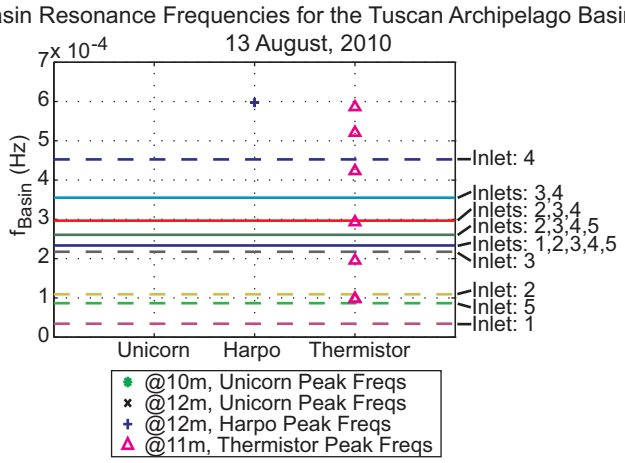

Fig. 16. Basin resonance frequencies, compared to peak frequencies from the AUVs' and thermistor's temperature spectra near the thermocline. The lines represent the Basin resonant frequencies of the Tuscan Archipelago basin based on the estimated basin surface area of $A_{surf} = 3880$ km^2. Each line accounts for a different subset of inlets to the basin in order to determine which inlets play a dominant role in the Basin resonance. The shaped markers highlight the temperature spectra peak frequencies in the Basin resonance range detected in the Unicorn, Harpo, and thermistor thermocline data. Note that Unicorn detected no frequencies near the Basin resonance. Also note that the calculated Basin frequencies may shift depending on the estimate of the basin surface area. Thus, the thermistor markers tend to align with different neighboring Basin frequencies if the surface area is estimated differently.

$A_{surf} = 3880$ km^2, we see an alignment with the resonant frequency imparted by inlets 2, 3, and 4 combined (see Fig. 16). This alignment is not surprising, given that inlets 2, 3, and 4 are the widest inlets and are the inlets most exposed to flows through deep channels outside the Tuscan Archipelago basin. This implies that inlets 2, 3, and 4 would be the most likely combined driving force for Basin resonance, and our data agrees.

V. Looking Ahead

Future work relating to this data set includes attempting to tease out the general direction of internal wave propagation from the AUVs' temperature data when divided into the five separate headings (one for each leg of the pentagonal loiter). If the peak frequencies of the temperature spectra increase or decrease slightly as the heading changes, the highest observed frequencies will correspond to the AUV heading nearly opposite of the direction of internal wave propagation, and the lowest observed frequencies will correspond to the AUV heading nearly perpendicular to the direction of internal wave propagation. If the phase speed of the internal waves (propagating

as a soliton or a larger group of waves) is on the order of the speed of the AUVs or less, as seen in this experiment, the AUVs most likely intersected the internal waves enough times at each of the 5 headings to be able to solve this problem. However, this may prove an unsolvable challenge in the case of swiftly (>10 m/s) propagating internal wave solitons, since solitons would only briefly appear in the AUV data.

In addition, internal wave amplitude may be estimated by examination of the depth variation of isotherms, particularly those concentrated near the thermocline depth in shallow water. As an internal wave passes a given point in the horizontal plane, the isotherms near the thermocline will rise or drop in depth by some distance indicative of the amplitude of the internal wave. To collect a proper data set for such a measurement, an AUV must collect temperature data in the depth range around the thermocline as the internal waves pass by. This is done (using our autonomy setup) by employing the adaptive thermocline tracking behavior as Unicorn did in Mission 2 of the Internal Wave Detection Experiment. This will be examined in a later work.

It would also be ideal to have another chance to execute all three missions of the Internal Wave Detection Experiment, again with at least two AUVs. We would like to collect environmental data sets for all three missions similar to those already collected, but over longer missions such that multiple hours or days worth of environmental data could be examined for persistent and / or longer period internal waves (including any tidal effects). Also, the goal of Mission 3 was to have the AUVs coordinated in motion (particularly coordinated in heading) through autonomous collaboration but spatially distributed in the horizontal plane such that internal wave speed could be directly estimated from the time it takes a wave crest to pass between the two AUVs on the same heading. Further analysis of data from Missions 1 and 2 in this experiment may reveal similar results for the sections of each loiter leg in which both Unicorn and Harpo have the same heading.

Finally, it will be important to quantify the hysteresis between the temperature and pressure sensors on Unicorn while yo-yoing. At the very least, a corrective adjustment should be made in the future to the resulting data sets. This will include accounting for the position difference between the CT sensor in the center section of Unicorn and the pressure sensor in its aft section (about 1.5 m away) and matching Unicorn's temperature values as it passed through the 12 m depth (during Mission 2) to those of Harpo at 12 m (also accounting for the fact that Unicorn was about 150 m behind Harpo).

VI. CONCLUSION

This paper is centered around the Internal Wave Detection Experiment using AUVs in the Tuscan Archipelago basin that took place on 13 August, 2010. Experiment design, hardware and code for implementation, resulting field trials, and post-deployment data results and analysis are discussed. This experiment took a novel approach to internal wave detection by tasking two autonomously collaborating AUVs to autonomously adapt their motion in relation to each other and to their dynamic environment, resulting in greater efficiency of sampling given a restrictive mission duration and in collection of fully synoptic data sets capturing internal waves.

The Internal Wave Detection Experiment involved two AUVs running the MOOS autonomy system guided by the IvP Helm. These AUVs used acoustic communication during the experiment to send and receive real-time data and status updates, which they used to autonomously coordinate their motions in the horizontal plane through a track-and-trail behavior. In the vertical axis, the Unicorn AUV autonomously adapted to changes in the environment while the Harpo AUV (which would have also adapted if the thermocline depth allowed for more reliable acoustic communication) swam just below the thermocline. A thermistor chain was also deployed for the duration of the experiment.

In examining the resulting AUV and thermistor data sets from this experiment, there is strong evidence of internal wave propagation along the thermocline near the buoyancy frequency of the thermocline interface ($N_{max} = 0.05747$ rad/s). Internal waves with nearly identical and lower frequencies were seen in the Unicorn, Harpo, and thermistor data collected near the thermocline depth. The 12 m AUV and 11 m thermistor results suggest the presence of buoyancy-supported internal waves along the thermocline (about 11 m depth) in the AUV operation region throughout the day on 13 August, 2010. This conclusion may also be extrapolated to say that internal waves are likely detectable along the thermocline throughout the rest of the Tuscan Archipelago basin during the summer, when the thermocline is fairly well defined. Given the lack of previous literature regarding internal waves in the Tuscan Archipelago basin, this finding is rather significant to the scientific groups that conduct acoustic (and other) experiments in this region.

Internal waves due to Basin resonance (a concept similar to Helmholtz resonance) in the basin were also examined. The results suggest that both single inlets and combinations of inlets

(see Fig. 1 and 16) excite internal wave frequencies within the basin that are detectable by a thermistor chain (and AUVs) deployed for long (multi-hour) missions. However, it is likely that inlets 2, 3, and 4 combined contribute a stronger resonance to the internal waves in the basin due to deep topography and currents just outside these basin inlets. This point is reinforced by the close alignment of one thermistor-detected frequency with the Basin resonance frequency from inlets 2, 3, and 4 combined. This supports the theory of the presence of low-frequency internal waves due to Basin resonance in the Tuscan Archipelago basin.

Overall, this experiment was novel in its use of multiple AUVs collaborating autonomously with each other and autonomously collecting environmentally-adaptive data sets for more synoptic spatiotemporal data coverage. Not only does this increase the efficiency of data collection (environmentally-adaptive autonomy behaviors allow us to collect the exact data set we need without a human in the loop), but the the ability to collect the specific data set a scientist is interested in by using AUVs running autonomy. The use of intelligent acoustic communication networking also allows the AUV operators and scientists to monitor (from the topside on a ship or shore) the data collected in near real time. These abilities are invaluable when ship time for data collection is so expensive, and we hope that improvements in AUV autonomy, adaptive environmental sampling techniques, and acoustic communications will allow us to further reduce necessary ship time for scientists and engineers to collect the specific data sets they need in the future.

ACKNOWLEDGMENT

The authors would like to acknowledge the NATO Undersea Research Centre (NURC) in La Spezia, Italy, for all their help in organizing and conducting field trials (GLINT ‘10) to test AUV feature tracking behaviors and conduct the Internal Wave Detection Experiment, as well as for use of their OEX AUV and research vessels that allowed us to collect the data sets necessary for this research. In particular, we would like to thank Marco Mazzi (NURC) for preparation and use of the OEX, Francesco Baralli (NURC) for setting up and running the OEX’s autonomy system, Kim McCoy (NURC) for numerous discussions on internal waves and his aid in the design of this experiment, and Toby Schneider (MIT LAMSS) for multi-AUV integration and always keeping things running smoothly in Unicorn’s autonomy system. Finally, we would like to thank the rest of the LAMSS group at MIT for their support of these efforts and the anonymous

reviewers for their very helpful feedback in revising this paper.

REFERENCES

[1] N. P. Fofonoff and R. C. Millard, "Algorithms for computation of fundamental properties of seawater," *Unesco technical papers in marine science*, vol. 44, 1983. [Online]. Available: http://unesdoc.unesco.org/images/0005/000598/059832eb.pdf

[2] J. S. Turner, *Buoyancy Effects in Fluids*, ser. Cambridge Monographs on Mechanics and Applied Mathematics. Cambridge University Press, 1973.

[3] J. Rodenas and R. Garello, "Internal wave detection and location in sar images using wavelet transform," *Geoscience and Remote Sensing, IEEE Transactions on*, vol. 36, no. 5, pp. 1494 –1507, sep 1998.

[4] R. F. Gasparovic, R. K. Raney, and R. C. Beal, "Ocean remote sensing research and applications at apl," Johns Hopkins APL, Tech. Rep. 4, 1999. [Online]. Available: http://www.jhuapl.edu/techdigest/TD/td2004/gaspar.pdf

[5] P. Brandt, A. Rubino, W. Alpers, and J. O. Backhaus, "Internal waves in the strait of messina studied by a numerical model and synthetic aperture radar images from the ers 1/2 satellites," *Journal of Physical Oceanography*, vol. 27, no. 5, pp. 648–663, 1997.

[6] B. D. Dushaw, "A review of internal tide observations by acoustic tomography and altimetry," in *Proceedings of the 5th Pacific Ocean Remote Sensing Conference (PORSEC)*, vol. 2, Goa, India, December 2000, pp. 651–652. [Online]. Available: http://staff.washington.edu/dushaw/

[7] A. R. Osborne and T. L. Burch, "Internal solitons in the andaman sea," *Science*, vol. 208, no. 4443, pp. pp. 451–460, 1980. [Online]. Available: http://www.jstor.org/stable/1683264

[8] P. Baines, "Satellite observations of internal waves on the australian north-west shelf," *Marine and Freshwater Research*, vol. 32, no. 3, pp. 457–463, 01 1981. [Online]. Available: http://www.publish.csiro.au/paper/MF9810457

[9] Y. Zhang, A. Baggeroer, and J. Bellingham, "Spectral-feature classification of oceanographic processes using an autonomous underwater vehicle," *Oceanic Engineering, IEEE Journal of*, vol. 26, no. 4, pp. 726 –741, October 2001.

[10] F. Cazenave, "Internal waves over the continental shelf in south monterey bay," Master's thesis, San Jose State University, 2008, paper 3506. [Online]. Available: http://scholarworks.sjsu.edu/etd_theses/3506

[11] M. Astraldi and G. P. Gasparini, *Seasonal and Interannual Variability of the Western Mediterranean Sea*, ser. Coastal and Estuarine Studies. Washington, D. C.: AGU, 1994, vol. 46, ch. 7: The Seasonal Characteristics of the Circulation in the Tyrrhenian Sea.

[12] S. Marullo, R. Santoleri, and F. Bignami, *Seasonal and Interannual Variability of the Western Mediterranean Sea*, ser. Coastal and Estuarine Studies. Washington, D. C.: AGU, 1994, vol. 46, ch. 8: The Surface Characteristics of the Tyrrhenian Sea: Historical Satellite Data Analysis.

[13] R. Santoleri, E. Böhm, and M. E. Schiano, *Seasonal and Interannual Variability of the Western Mediterranean Sea*, ser. Coastal and Estuarine Studies. Washington, D. C.: AGU, 1994, vol. 46, ch. 9: The Sea Surface Temperature of the Western Mediterranean Sea: Historical Satellite Thermal Data.

[14] T. Schneider and H. Schmidt, "The Dynamic Compact Control Language: A compact marshalling scheme for acoustic communications," in *Proceedings of the IEEE Oceans Conference 2010*, Sydney, Australia, May 2010.

[15] Goby Developers, "Goby underwater autonomy project documentation." [Online]. Available: http://gobysoft.com/doc/1.0

[16] M. R. Benjamin, H. Schmidt, P. M. Newman, and J. J. Leonard, "Nested autonomy for unmanned marine vehicles with MOOS-IvP," *Journal of Field Robotics*, vol. 27, no. 6, pp. 834–875, 2010. [Online]. Available: http://dx.doi.org/10.1002/rob.20370

[17] M. R. Benjamin, J. J. Leonard, H. Schmidt, and P. M. Newman, "An overview of MOOS-IvP and a brief users guide to the IvP Helm autonomy software," MIT, Tech. Rep. MIT-CSAIL-TR-2009-028, 2009. [Online]. Available: http://hdl.handle.net/1721.1/45569

[18] P. Kundu and I. Cohen, *Fluid Mechanics*. Academic Press, 2008.

[19] S. Petillo, H. Schmidt, and A. Balasuriya, "Constructing a distributed auv network for underwater plume-tracking operations," *International Journal of Distributed Sensor Networks: Special Issue on Distributed Mobile Sensor Networks for Hazardous Applications*, 2012, in press.

[20] S. Kemna, M. Hamilton, D. Hughes, and K. LePage, "Adaptive autonomous underwater vehicles for littoral surveillance," *Intelligent Service Robotics*, vol. 4, pp. 245–258, 2011, 10.1007/s11370-011-0097-4. [Online]. Available: http://dx.doi.org/10.1007/s11370-011-0097-4

[21] Woods Hole Oceanographic Institution, "WHOI Acoustic Communications: Micro-Modem Overview," accessed 24 August, 2011. [Online]. Available: http://acomms.whoi.edu/umodem/

[22] T. Schneider, "Google Earth interface for Ocean Vehicles (GEOV)." [Online]. Available: http://aubergine.whoi.edu/geov/index.php

[23] S. Petillo, A. Balasuriya, and H. Schmidt, "Autonomous adaptive environmental assessment and feature tracking via autonomous underwater vehicles," in *Proceedings of the IEEE Oceans Conference 2010*, Sydney, Australia, May 2010.

[24] K. V. MacKenzie, "Nine-term equation for the sound speed in the oceans," *The Journal of the Acoustical Society of America*, vol. 70, no. 3, pp. 807–812, September 1981.

[25] "MicroCAT C-T (P optional) Sensor SBE 37-SI." [Online]. Available: http://www.seabird.com/products/spec_sheets/37sidata.htm

[26] "Google Earth." [Online]. Available: http://earth.google.com/ocean/

Stephanie Petillo is an Oceanographic Engineering Ph.D. candidate in the Massachusetts Institute of Technology / Woods Hole Oceanographic Institution Joint Graduate Program. She received her B.S. degree in Aerospace Engineering with a minor in Italian Language and Culture from the University of Maryland - College Park in 2008, and has been in the MIT / WHOI Joint Graduate Program from 2008 to present. Ms. Petillo's research has focused on using autonomous underwater vehicles (AUVs) to perform autonomous and environmentally adaptive sampling of the ocean environment, focusing on underwater feature detection and tracking for more efficient and synoptic data collection with AUVs.

Henrik Schmidt is Professor of Mechanical & Ocean Engineering at the Massachusetts Institute of Technology. He received his MS degree from The Technical University of Denmark in 1974, and his Ph.D. from the same institution in 1978. Following a post-doctoral fellowship at the Risoe National Laboratory in Denmark, he joined the NATO Undersea Research Centre in Italy in 1982, where he worked until he joined the MIT faculty in 1987. Professor Schmidt's research has focused on underwater acoustic propagation and signal processing, and most recently on the development of environmentally adaptive acoustic sensing concepts for networks of autonomous underwater vehicles. Prof. Schmidt is a Fellow of the Acoustical Society of America, and he is the 2005 recipient of the ASA *Pioneers of Underwater Acoustics Medal*.